Surface Engineering

ISSN: 0267-0844 (Print) 1743-2944 (Online) Journal homepage: http://www.tandfonline.com/loi/ysue20

Robust hydrophobic coating on glass surface by an atmospheric-pressure plasma jet for plasma-polymerisation of hexamethyldisiloxane conjugated with (3-aminopropyl) triethoxysilane

Md. Mokter Hossain, Quang Hung Trinh, Duc Ba Nguyen, M. S. P. Sudhakaran & Young Sun Mok

To cite this article: Md. Mokter Hossain, Quang Hung Trinh, Duc Ba Nguyen, M. S. P. Sudhakaran & Young Sun Mok (2018): Robust hydrophobic coating on glass surface by an atmospheric-pressure plasma jet for plasma-polymerisation of hexamethyldisiloxane conjugated with (3-aminopropyl) triethoxysilane, Surface Engineering, DOI: 10.1080/02670844.2018.1524037

To link to this article: https://doi.org/10.1080/02670844.2018.1524037

Published online: 26 Sep 2018.

SURFACE ENGINEERING
https://doi.org/10.1080/02670844.2018.1524037

The Institute of Materials, Minerals and Mining

Taylor & Francis
Taylor & Francis Group

Robust hydrophobic coating on glass surface by an atmospheric-pressure plasma jet for plasma-polymerisation of hexamethyldisiloxane conjugated with (3-aminopropyl) triethoxysilane

Md. Mokter Hossain[a], Quang Hung Trinh[b,c], Duc Ba Nguyen [a], M. S. P. Sudhakaran[a] and Young Sun Mok[a]

[a]Department of Chemical and Biological Engineering, Jeju National University, Jeju, Korea; [b]Institute of Research and Development, Duy Tan University, Da Nang, Vietnam; [c]Faculty of Mechanical Engineering, Le Quy Don Technical University, Hanoi, Vietnam

ABSTRACT

Plasma polymerisation of hexamethyldisiloxane (HMDSO) and (3-aminopropyl)triethoxysilane (APTES) was attempted to form a robust hydrophobic coating film on glass surface. Although HMDSO is a common precursor for generating hydrophobic surface, the HMDSO-polymerised thin film is poor in strength. For the purpose of achieving the mechanical robustness of the coating, APTES was used together with HMDSO. Plasma polymerisation was performed using a dielectric barrier discharge plasma jet by varying the ratio of the two precursors to find a suitable condition that would produce robust hydrophobic thin film. Various instrumental techniques were used to characterise the coating layer. As a result of the examination of the hydrophobicity through the water contact angle measurements and the robustness by the scratch tests, the most reasonable coating was achieved at the HMDSO/APTES ratio of 3/1, the voltage of 7 kV and the treatment time of 60 s, and at this condition the WCA was 143°.

ARTICLE HISTORY
Received 12 July 2018
Revised 6 September 2018
Accepted 10 September 2018

KEYWORDS
HMDSO; APTES; plasma jet; thin film; robust coating

Introduction

Nonthermal plasma (NTP) treatment at atmospheric pressure has been a warm research topic in recent years for making hydrophobic surface of various materials [1–7]. The hydrophobic surface can be used for various purposes such as self-cleaning windows, anti-icing, out-door textiles, self-cleaning of antennas, ultra-dry surface applications, protection of circuits and grids, medical devices, and other optical apparatuses [8–12]. Basically, the thin films deposited by plasma polymerisation are pinhole free, have good adhesion, and have better mechanical and chemical stabilities. To get hydrophobic characteristics the surface requires nano- to micro-scale roughness. Both the surface roughness and the surface chemistry affect the hydrophobicity [2]. Up to now, several methods have been proposed to generate surface roughness, including plasma treatment, sol–gel deposition, anodisation, electrodeposition, chemical treatment, hot-water immersion, and lithography [12–17]. A surface having water contact angle (WCA) from 90° to 150° is known as hydrophobic, and the surface more than 150° is known as super hydrophobic due to its excellent self-cleaning ability.

Although low surface energy materials such as fluorocarbons can be used to produce hydrophobic coatings [14,18,19], the plasma polymerisation of silicon-based compounds is more environmentally friendly. This study has dealt with the plasma polymerisation of hexamethyldisiloxane (HMDSO, $C_6H_{18}OSi_2$) and (3-aminopropyl)triethoxysilane (APTES, $H_2N(CH_2)_3Si(OC_2H_5)_3$) at atmospheric pressure. The main purpose of using the two precursors is to increase not only hydrophobicity but also robustness of the coating. As well known, one of the major drawbacks of the silicon compound coatings is their poor mechanical abrasion which extinguishes the self-cleaning function due to the damage of surface roughness and coating layer. HMDSO is generally used to promote hydrophobicity, but due to its poor adhesion to metal or inorganic material, the long-term stability of the coating layer is not satisfactory. Hence, APTES is used with HMDSO to overcome this issue but the cost is to sacrifice the WCA as it is known that APTES is hydrophilic in nature. Basically, organosilane reagents are commonly used to produce functionalised thin films on silicon oxide and other substrates for a variety of technological applications. APTES is one of the similar aminosilanes which is used in this study to facilitate production of arrays of metal nanoparticles on silica substrates [20]. For surface coating, APTES is highly suggested to use for its covalent attaching to silica (SiO_2), titania (TiO_2), organic films, and metal oxides [2]. Masuko et al. [21] studied the shear strength and durability of self-assembled monolayer (SAM) and the tribological performance with different numbers of siloxane bonds on smooth silicon substrates. They found that increasing the number of siloxane bonds of SAMs

CONTACT Young Sun Mok smokie@jejunu.ac.kr Department of Chemical and Biological Engineering, Jeju National University, Jeju 63243, Korea

gives more stable surface with low friction and greater durability. One of the key parameters explored in this work was the ratio of HMDSO to APTES.

Experimental

Schematic diagrams of the plasma polymerisation system and homemade scratch tester are shown in Figure 1. The plasma reactor was made of a glass tube and two stainless steel needles acting as the high voltage (HV) electrode. The HV electrode was powered by an AC power source (Korea Switching Co.) with an operating frequency of 11.5 kHz. The inner and outer diameter of the glass tube was 5.0 and 8.0 mm, respectively. The distance between HV electrode tip and the end of the reactor glass tube was kept constant at 75 mm. The gap between the end of the tube and the substrate was kept constant at 2 mm. The substrate samples held on a Teflon plate reciprocated below the stationary plasma jet at a speed of 90 mm s^{-1}. Argon (99.99%) and nitrogen (99.99%) were used as the carrier and shielding gas, and they were separately fed into the system as shown in Figure 1(a). The purpose of using the shielding gas was to protect the plasma jet from the interference of oxygen and water vapour diffused from ambient air. The two precursors, namely, HMDSO and APTES were purchased from Sigma-Aldrich Korea Co., Ltd. HMDSO was used to promote hydrophobicity while APTES to promote mechanical robustness.

The appropriate condition was determined based on the parametric study with several key parameters such

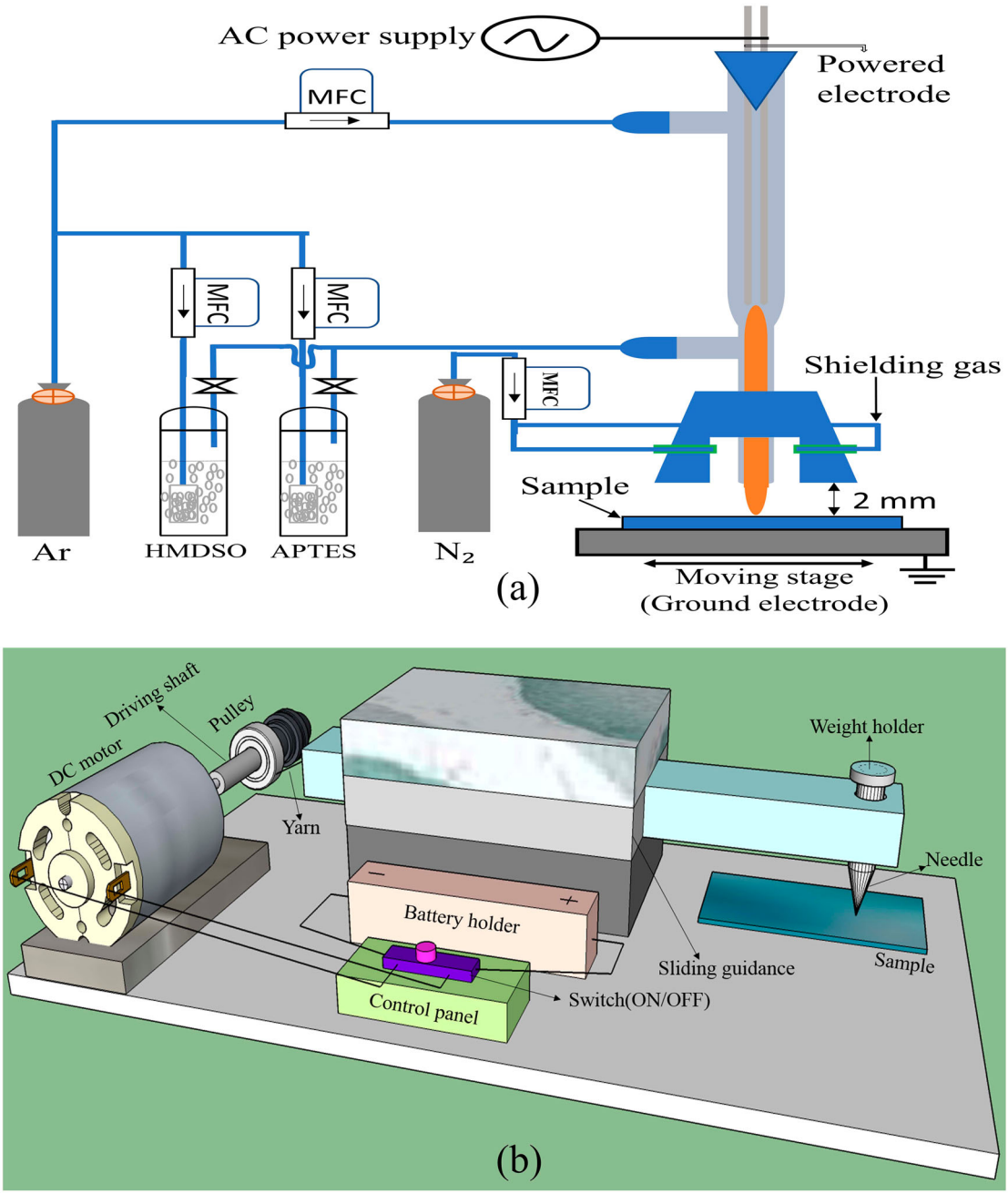

Figure 1. Schematic diagrams of (a) the experimental setup and (b) homemade scratch tester.

as treatment time, applied voltage, gas flow rate, and the ratio of two precursors. The treatment time was changed from 30 to 120 s, and the effect of applied voltage was examined from 5 to 8 kV. The total concentration of the precursors was set to 280 ppm (parts per million, volumetric). The concentration of HMDSO was 280 ppm in the HMDSO-alone case (H100); in the APTES-alone case (A100), the concentration was also the same. The HMDSO/APTES (H/A) ratio was varied by 3/1, 1/1, and 1/3. Both precursors were delivered to the jet by bubbling HMDSO and APTES (at 25° and 121°C, respectively) contained in Pyrex flasks using argon gas. The flow rate of the shielding gas was fixed at 2.5 L/min, and the effect of the flow rate of argon on the coating was examined in the range of 0.5–4.5 L/min. Thus, the total flow rate of argon and nitrogen was changed from 3.0 to 7.0 L/min. The substrates for coating were soda-lime glasses with dimensions of 75 mm × 27 mm × 1.2 mm, and thus the resulting coated area was estimated to be around 1500 mm^2.

The WCA of the coated surfaces was measured for understanding the hydrophobicity of the coated surface polymer. The WCA measurements were carried out on a goniometer (Phonix 300, Surface & Electro Optics Co., Ltd., Korea) using sessile drop technique by dropping about 10 µL of distilled water on the sample's surfaces. The surface morphology was seen by scanning electron microscopy (SEM, JSM-6700F, JEOL, Japan) at an operating voltage of 15 kV. The surface nanostructures of the coating were examined by atomic force microscopy (AFM, Nano Xpert II, EM4SYS, USA). Fourier transform infrared spectroscopy (FTIR, FTIR-7600, Lambda Scientific, Australia) was used to investigate the composition of the effluent from the plasma jet and the deposited thin films. The coating surface chemistry was analysed using X-ray photoelectron spectroscopy (XPS). The coating layer robustness was performed by homemade scratch tester and wear tracks were observed by an optical microscope (2MP 1000X 8 LED USB Digital Microscope Endoscope Zoom Camera, A4Tech, Taiwan). For a typical scratch test, a diamond tip moves over the surface to make a scratch with either constant or progressively increasing load [22]. Usually, the normal force, tangential force, friction coefficient, acoustic emission, and penetration depth are measured continuously during scratch testing [22]. Figure 1(b) shows the home-made scratch tester used in this work to examine the robustness of the coating. The scratch tester is mainly composed of a dc motor which drives a needle (tip diameter: 0.5 mm) to move on the sample's surface for creating scratch with predetermined vertical loads. Yarn is used to connect motor's driving shaft to the needle holder. The needle holder is guided by a sliding guide and it can travel horizontally back and forth. The samples for testing were put under the tip of the needle and fixed by double sided tape so that the samples did not move during scratching. The tip of the needle was cleaned with ethanol and tissue wiper before and after a scratch test for each sample. The moving speed of the tip was set to 37 mm s^{-1} and the length of scratch was around 10 mm. For every sample, constant loads were applied every time to determine the breakdown force for the coating layer.

Results and discussion

Water contact angle measurements of the glass substrates

The surfaces with different degrees of hydrophobicity were observed after the plasma polymerisation process, depending on the operating conditions including the applied voltage, the gas flow rate, the HMDSO/APTES (H/A) ratio, and the treatment time. Figure 2 shows the dependence of WCA on the treatment time, the applied voltage, the H/A ratio and the gas flow rate. The WCA results reported in Figure 2 are the average values of five measurements at each condition. In detail, Table 1 summarises the values of the experimental parameters, the average WCAs and the standard deviations.

The effect of treatment time was examined from 30 to 120 s at a H/A ratio of 3/1 with the applied voltage and the total gas flow rate kept constant at 7 kV and 6 L/min, respectively. As shown in Figure 2(a), the WCA was varied from 100° to 141° by changing the treatment time within the investigated range. Basically, WCA depends on surface roughness and thickness. At a short treatment time of 30 s, the surface roughness and coverage were relatively poor, compared with 45–120 s treatment time. Increasing the treatment time can allow more deposition on the surface, which increases thickness, surface coverage and roughness. After a certain limit, however, thickness may increase but surface coverage and roughness remain similar and hence the WCA does not increase. In this experiment, the WCA increased from 100° to 143° with increasing the treatment time from 30 to 60 s, but further increasing the treatment time hardly affected the WCA. Thus, 60 s was chosen for the treatment time.

In the second step, the effect of applied voltage was examined from 5 to 8 kV with the treatment time, the H/A ratio, and the total flow rate kept constant at 60 s, 3/1, and 6 L/min, respectively. As in Figure 2(b), the WCA increased with raising the applied voltage from 5 to 7 kV and then levelled off. Generally, the higher the applied voltage, the more intense the plasma was, leading to the enhancement in the deposition rate and the formation of particulates in the plasma gas phase, called dusty plasma which is prerequisite to obtain rough surfaces. The highest WCA were

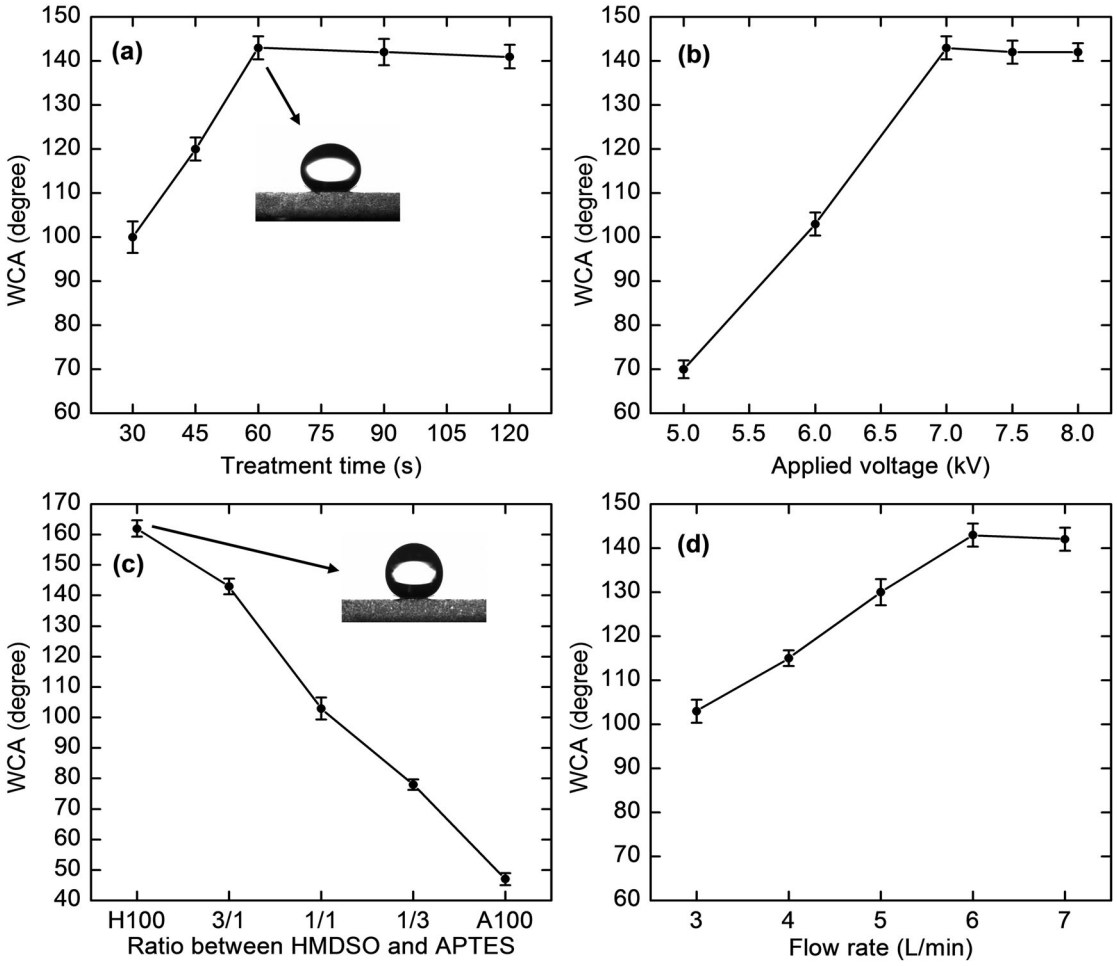

Figure 2. Dependence of WCA on (a) the treatment time, (b) the applied voltage, (c) the H/A ratio and (d) the gas flow rate.

measured to be 143° at 7 kV. There was no significant change in the WCA at higher applied voltages. From the results obtained, the applied voltage of 7 kV was chosen for the appropriate applied voltage.

The third step was to see the effect of the H/A ratio on the WCA. The treatment time and the applied voltage chosen above were 60 s and 7 kV, respectively. Figure 2(c) shows the dependence of WCA on the H/A ratio with the treatment time and applied voltage kept constant at 60 s and 7 kV, respectively. The WCA values of the coatings formed from the single precursor of APTES and HMDSO are also added for the purpose of comparison. It is natural that the WCA should decrease with increasing the content of APTES in the mixture of the two precursors due to its hydrophilic character, which has been confirmed by the low WCA of the A100 coating.

Lastly, the gas flow rate was changed to understand its effect on the WCA while the treatment time, the applied voltage, the H/A ratio were kept constant at 60 s, 7 kV, and 3/1, respectively. In Figure 2(d), it was observed that by increasing the total gas flow rate from 3 to 6 L/min the plasma was getting more intense, leading to an increased WCA from 103° to 143°. But further increases of the feed gas flow rate to 7 L/min did not noticeably change the WCA, and hence 6 L/min was chosen for the optimal gas flow rate.

Table 1. Operating conditions and WCA measurement results.

Treatment time (s)	Applied voltage (kV)	H/A ratio (–)	Gas flow rate (L min^{-1})	Average WCA (°)	Standard deviation
30	7.0	3/1	6	100	2.4
45	7.0	3/1	6	120	2.1
60	7.0	3/1	6	143	2.6
90	7.0	3/1	6	142	2.4
120	7.0	3/1	6	141	2.1
60	5.0	3/1	6	70	2.5
60	6.0	3/1	6	103	2.7
60	7.0	3/1	6	143	2.6
60	7.5	3/1	6	142	2.8
60	8.0	3/1	6	142	2.7
60	7.0	H100	6	162	3.1
60	7.0	3/1	6	143	2.6
60	7.0	1/1	6	101	2.8
60	7.0	1/3	6	78	2.5
60	7.0	A100	6	47	2.1
60	7.0	3/1	3	103	2.7
60	7.0	3/1	4	115	2.2
60	7.0	3/1	5	130	2.3
60	7.0	3/1	6	143	2.6
60	7.0	3/1	7	142	2.6

Coating stability test

Coating stability was examined by performing natural and thermal aging. All the plasma-treated samples

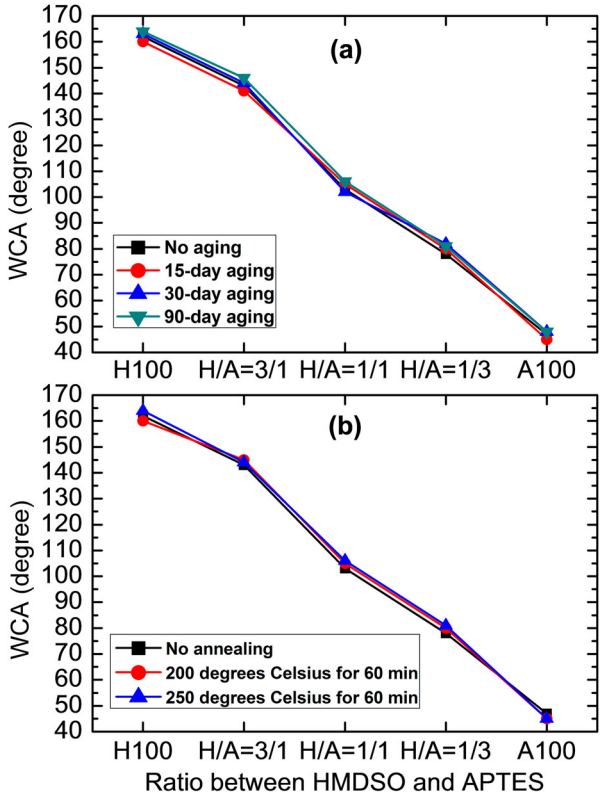

Figure 3. (a) Aging time effect and (b) annealing temperature effect on the coating.

Table 2. Thickness and RMS roughness of each sample.

Sample	Thickness (nm)	RMS roughness (nm)
H100	420	182 ± 5
H/A = 3/1	370	123 ± 6
H/A = 1/1	317	86 ± 4
H/A = 1/3	275	48 ± 4
A100	215	36 ± 5

were stored in centrifuge tube at room temperature. The aging time was reported to have a significant effect on WCA for the powder substrate coating [23]. Trinh et al. [23] have reported that the WCA could increase by 15–40° within 30 days in the case of powder substrate coating. Unlike the power substrate coating, the WCA of the plasma-treated substrate (glass) as shown in Figure 3(a) was hardly affected by the aging (15, 30, and 90 days), indicating that the coating is highly stable and durable. The thermal stability of the coating was examined by annealing tests at 200°C and 250°C for one hour. The WCA did not nearly change in both cases, as shown in Figure 3(b).

Surface morphology and coating thickness

The AFM and SEM analyses were carried out to understand the relationship between the two precursors in the plasma polymerisation process as well as to see the surface morphology, roughness and thickness of the coating. Root-mean-square (RMS) roughness and coating thickness are listed in Table 2. Figure 4 shows the AFM results of the coated samples for H100, A100 and various H/A ratios. From the figure, it can be seen that the number of needle-like peaks grown on the substrate surfaces decreased from Figure 4(a–e). The higher the number of needle-like peaks, the higher the surface roughness. The H100-alone coating (Figure 4(a)) had the highest surface roughness and thickness and it is likely due to the hydrophobic nature and reactivity of HMDSO in the plasma. When HMDSO and APTES were added together, the roughness and coating thickness decreased as the H/A ratio decreased. The formation of rough surfaces with nanoscale topographic features results from the generation of particulates through gas-phase condensation reactions. The plasma-induced particulates then deposit and adhere to a substrate [5]. In the plasma polymerisation, it is believed that HMDSO is more

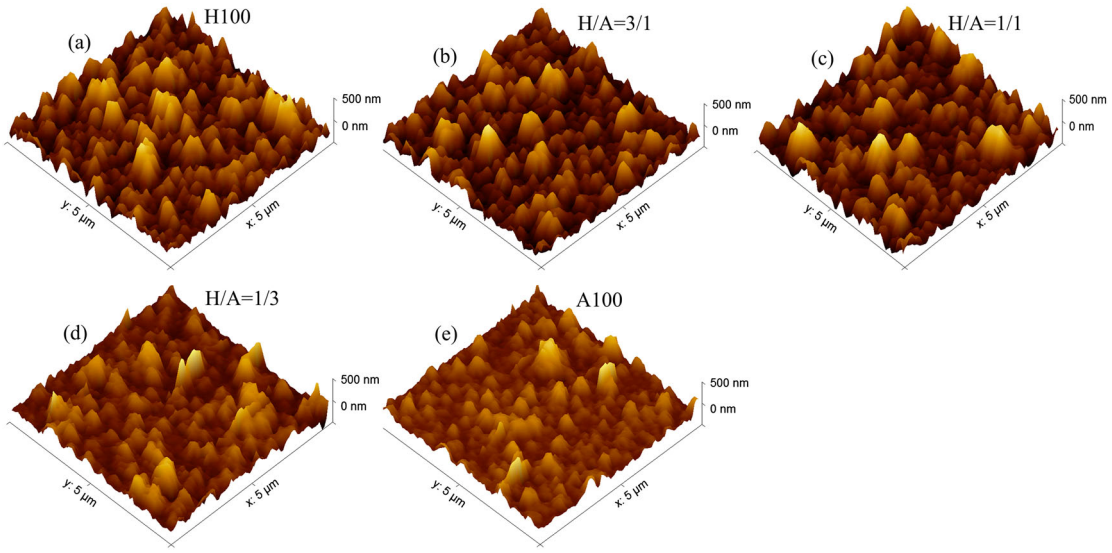

Figure 4. AFM images of the coated samples. (a) H100; (b) H/A = 3/1; (c) H/A = 1/1; (d) H/A = 1/3; (e) A100.

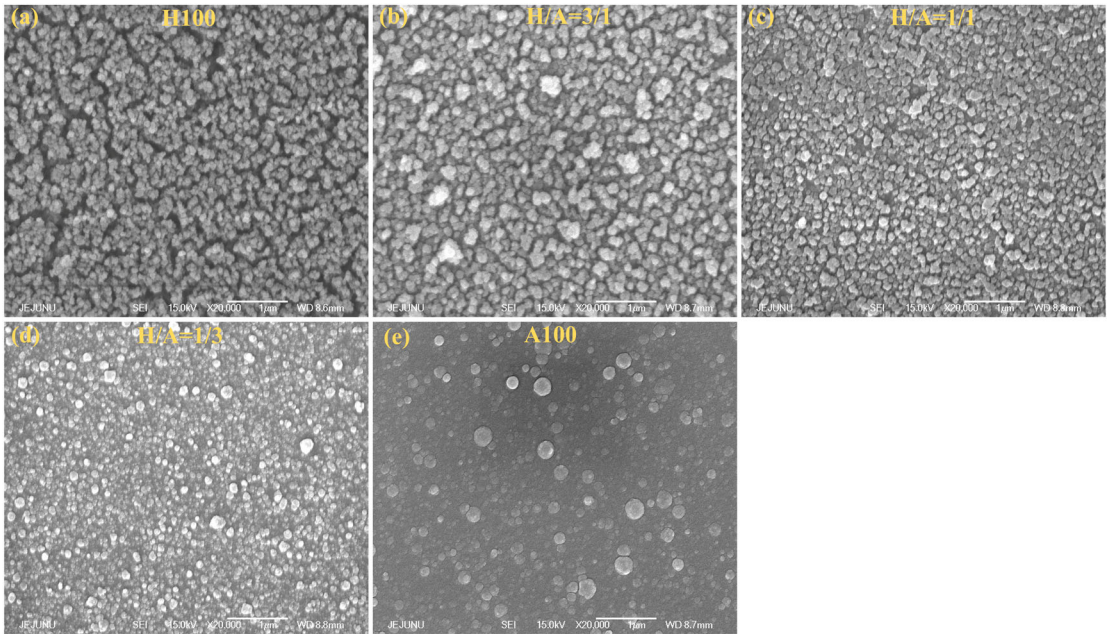

Figure 5. SEM images of the coated samples. (a) H100; (b) H/A = 3/1; (c) H/A = 1/1; (d) H/A = 1/3; (e) A100.

active than APTES to produce fragments, facilitating the formation of particulates and therefore the high surface roughness.

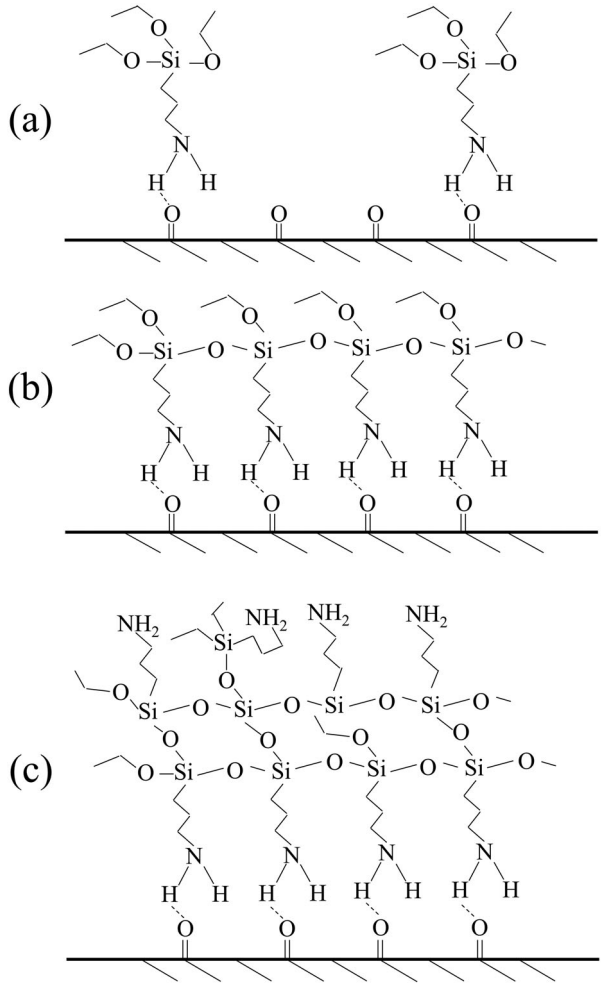

Figure 6. Surface modification and possible reaction routes of APTES: (a) hydrogen bonding due to initial adsorption, (b) surface attachment, and (c) multilayer formation.

Figure 5 shows SEM images of the corresponding samples. The coatings consist of nanostructures ranging from 70 to 200 nm. It was found that the coatings had shown cauliflower-like morphology in the case of H100 and the H/A ratio of 3/1 (Figure 5(a,b), respectively), while in the other cases the nanostructures formed were like numerous circular islands with different sizes.

Surface modification by APTES

Plasma polymerisation with amines is still under investigation and only a few articles discussed about this issue [24–28]. The plasma polymerisation by the APTES is described in Figure 6 [29–31]. For better understanding, the surface modification by the APTES can be divided into three parts: (a) hydrogen bonding due to initial adsorption, (b) surface attachment, and (c) multilayer formation [31]. If we take a careful look at Figure 6(a,b), it can be seen that still there is no sign of donor amine and acceptor groups. It indicates that some of APTES molecules are not H-bonded to the surface. Hence, the formation of siloxane cross-links depends on the inter-APTES reaction and makes a thin layer (Figure 6(c)) where donor amine and acceptor H-bond both are present.

FTIR spectroscopy

The chemical characterisations of the coatings were done by the FTIR spectroscopy, which are shown in Figure 7. Since the soda-lime glass is not transparent to infrared (IR), polymer films were deposited on potassium bromide (KBr) disks by the same plasma polymerisation process. All the spectra were collected by

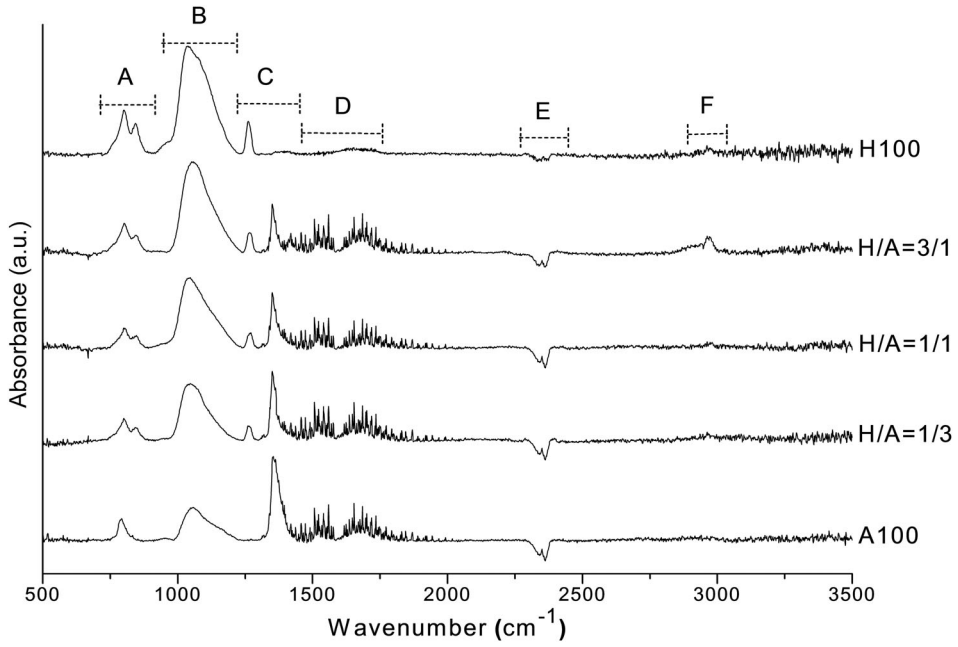

Figure 7. FTIR spectra of the coated samples from 500 to 3500 cm^{-1}.

taking average of 10 scans at 1 cm^{-1} resolution in the range of 500–3500 cm^{-1}. The asymmetric stretching band of the backbone Si–O–Si is found at 1047 cm^{-1} [32,7]. Si–O stretching in Si–OH can be seen at 830–940 cm^{-1} [7,33,34], and Si–C stretching is found at 800 cm^{-1} [7]. The Si–CH_3 symmetric deformation appears at 1260, 1350, and 2966 cm^{-1} where the peaks at 1260 and 1350 cm^{-1} are medium in intensity and the peak at 2966 cm^{-1} is weak in intensity [32,35]. The absorption band at 1600 cm^{-1} that corresponds to water is due to the moisture of KBr. Peaks from 2340 to 2360 cm^{-1} are due to the presence of CO_2 in the ambient environment [36].

XPS results

The XPS examination was done to understand the surface chemical composition and the chemical bonds of the polymer thin films. Figure 8 demonstrates the atomic concentrations measured by the XPS for various specimens. Three samples out of five were selected (H100, A100, and H/A = 3/1) for XPS analyses where all the three samples contain silicon (Si), carbon (C), oxygen (O), and nitrogen. The H100 sample has shown 37.5% of carbon, 33.5% of oxygen, 27.1% of silicon, and 1.9% of nitrogen. On the other hand, APTES (A100) and the H/A ratio of 3/1 coated sample have shown 20.9% and 40.2% of carbon, 50.1% and 37.9% of oxygen, 24.6% and 18.8% of silicon, and 4.4% and 3.1% of nitrogen, respectively. Here, sample H100 has shown less nitrogen when compared to the other two samples, which is due to no nitrogen from the precursor.

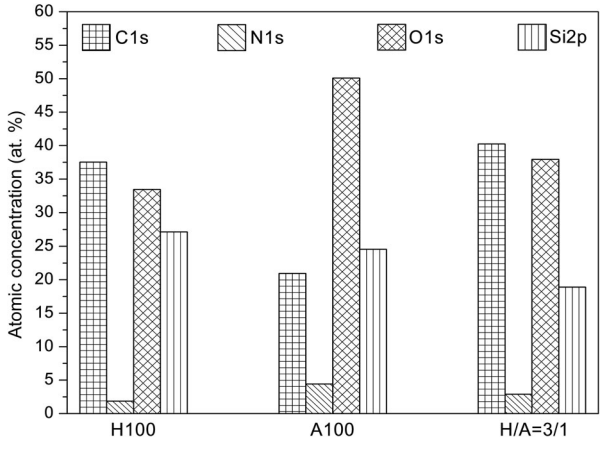

Figure 8. Atomic composition (%) of selected sample surfaces.

The deconvolution results of C1s spectra are presented in Figure 9 and Table 3. The plasma-polymerised thin film shows a high contribution of the Si–CH_x ($x = 3$ or 2) or C–C at 284.6 eV in the all three samples in Figure 9 [37,38]. The peaks at 286 and 287.5 eV are seen due to the presence of C–O or C–N and C=O in all the coated samples [37]. But, C–Si_x ($x = 3$ or 2) peak at 283.2 eV is found only in the sample H100 and H/A ratio of 3/1 in Figure 9 (a,c) [37]. So, it could be said that this chemical bond is generated due to the HMDSO precursor. On the other hand, the chemical bonding of O–C-O at 288.7 eV in Figure 9(b,c) is due to the APTES precursor [37].

UV-visible spectroscopy

Transmittance and hydrophobicity have an inverse relation because both depend on the thickness and roughness of the coating. As the surface thickness and roughness of the coating increase, the

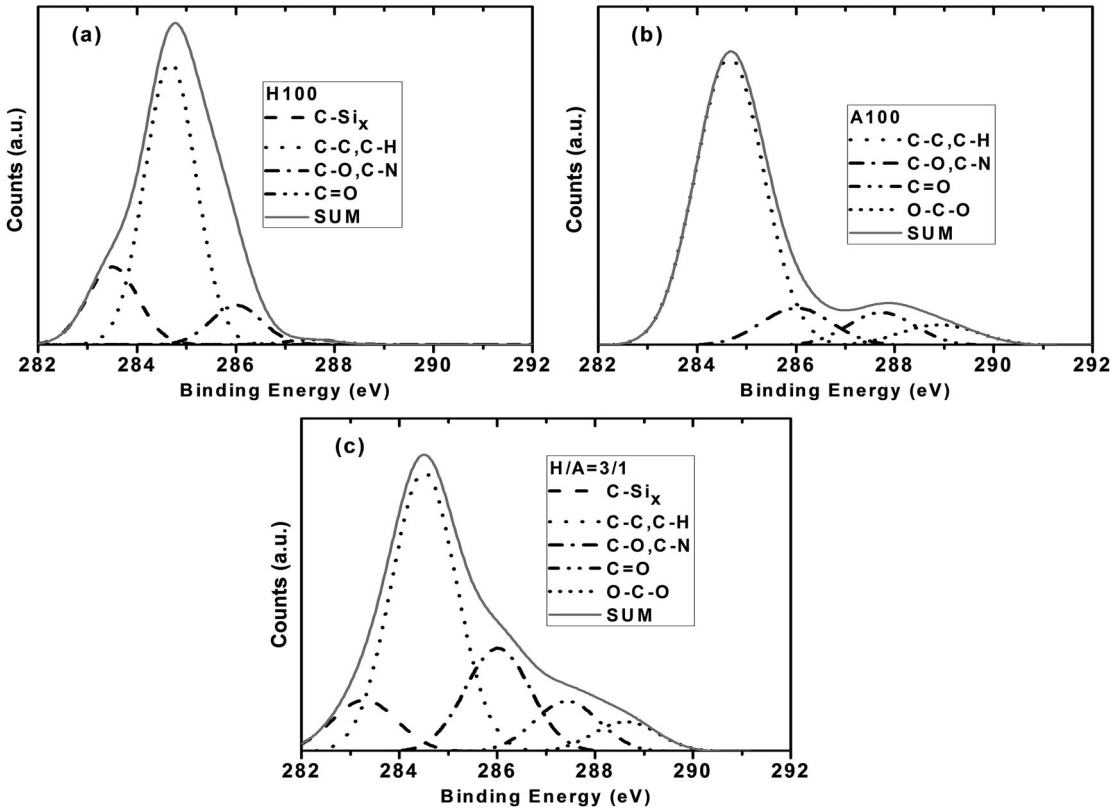

Figure 9. Deconvolution of C1s spectra (282–290 eV) of the selected coated samples.

Table 3. Deconvolution of C1s spectra along with binding energies and functional groups.

Functional groups	Peak position (eV)	References
C–Si$_x$ ($x = 3$ or 2)	283.2	[37]
Si–CH$_x$ ($x = 3$ or 2) or C–C	284.6	[37,38]
C–O or C–N	286	[37]
C=O	287.5	[37]
O–C–O	288.7	[37]

hydrophobicity increases but the visibility decreases [39]. Figure 10 shows the UV–VIS transmission spectra of the bare glass and the ones coated with HMDSO, APTES, and their mixture at various ratios [39]. Uncoated glass exhibited around 80% transmittance in the visible regions (from 390 to 700 nm), while the plasma-treated glasses at different H/A ratios exhibited slightly lower transmittance.

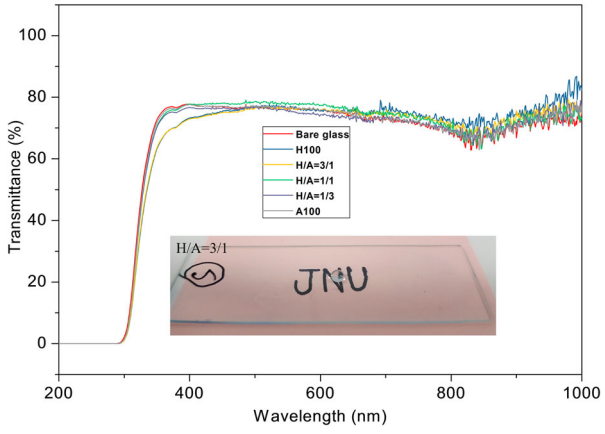

Figure 10. UV-visible spectra of the coated samples.

Table 4. Scratch test results for each sample.

Sample	Annealing temperature (°C)	Applied force (AF) (dyne)	Sliding speed (mm s^{-1})	Needle tip diameter (mm)
H100	250	3432	37	0.5
H/A = 3/1	250	9316	37	0.5
H/A = 1/1	250	13,239	37	0.5
H/A = 1/3	250	20,104	37	0.5
A100	250	25,007	37	0.5

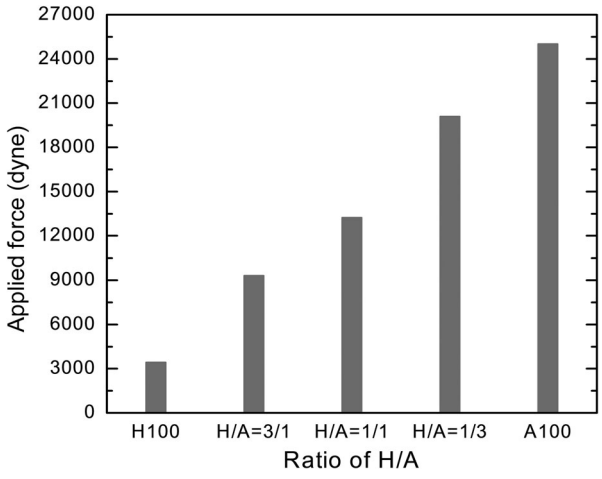

Figure 11. Breakdown forces of the samples obtained by the scratch tests.

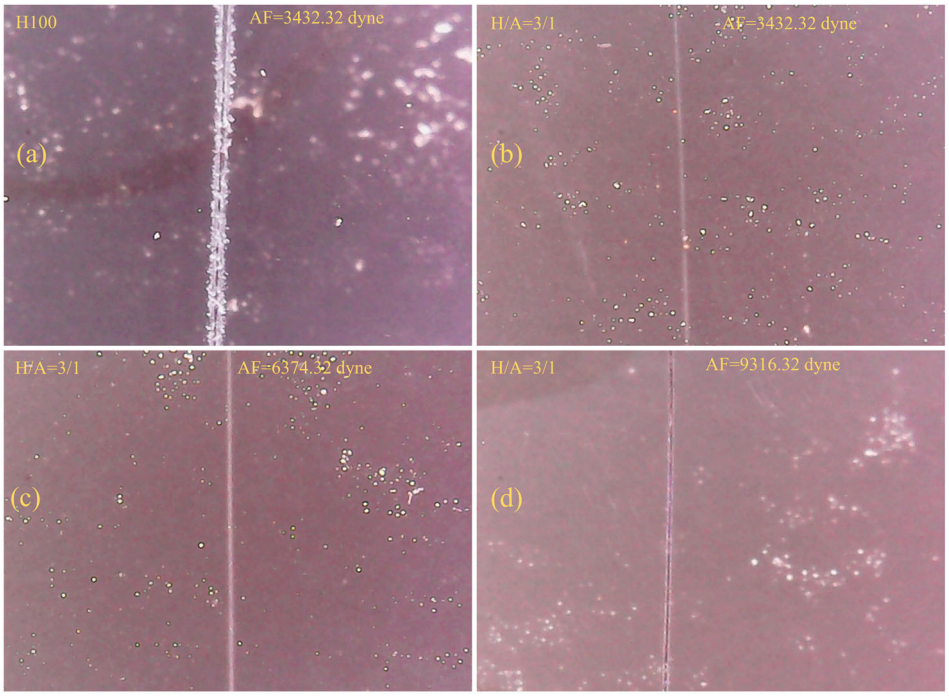

Figure 12. Microscope images of the selected samples.

Scratch tests

To analyse the mechanical robustness of the coatings, scratch tests were performed after the annealing of the samples at 250°C for 1 h. All the experimental conditions for the scratch test are summarised in Table 4. The weight of weight holder and needle was 3432 dyne, and thus the minimum applied force was 3432 dyne. The force was gradually increased to find the breakdown force. All the results of the scratch tests are shown in Figure 11, and the scratch test images taken by the digital microscope are given in Figure 12. The sample H100 could not sustain minimum force applied by the scratch tester. When the mixture of the two precursors was used, the coating was stronger as the H/A ratio decreased.

Conclusions

The plasma polymerisations of HMDSO and APTES at different ratios were carried out by the atmospheric-pressure plasma jet in order to get a robust and stable hydrophobic surface layer on the glass surface. The HMDSO was used to promote hydrophobicity and the APTES to promote robustness and durability owing to the presence of amines capable of promoting the adhesion of the coating layer. In terms of hydrophobicity and robustness of the coating, the applied voltage of 7 kV, treatment time of 60 s, and the H/A ratio of 3/1 were chosen as optimal condition. The WCA of 143° and reasonable mechanical strength were obtained under this condition. The deposition of the polymer thin film on the glass surface was evidenced by the SEM and AFM images. The UV–VIS transmission study revealed that there was no significant transmittance loss in the visible region for the sample with H/A ratio of 3/1. Consequently, the non-thermal atmospheric-pressure plasma jet could be a good candidate for producing reliable hydrophobic surface.

Disclosure statement

No potential conflict of interest was reported by the authors.

Funding

This work was supported by the 2017 Scientific Promotion Program funded by Jeju National University.

ORCID

Duc Ba Nguyen http://orcid.org/0000-0002-5018-6531

References

[1] Vogelsang A, Ohl A, Foest R, et al. Hydrophobic coatings deposited with an atmospheric pressure microplasma jet. J Phys D Appl Phys. 2010;43:485201.
[2] Genzer J, Efimenko K. Recent developments in superhydrophobic surfaces and their relevance to marine fouling: a review. Biofouling. 2006;22(5):339–360.
[3] Ladwig A, Babayan S, Smith M, et al. Atmospheric plasma deposition of glass coatings on aluminum. Surf Coatings Technol. 2007;201:6460–6464.
[4] Li X-M, Reinhoudt D, Crego-Calama M. What do we need for a superhydrophobic surface? A review on the recent progress in the preparation of superhydrophobic surfaces. Chem Soc Rev. 2007;36:1350–1368.

[5] Marchand DJ, Dilworth ZR, Stauffer RJ, et al. Atmospheric RF plasma deposition of superhydrophobic coatings using tetramethylsilane precursor. Surf Coatings Technol. 2013;234:14–20.
[6] Múgica-Vidal R, Alba-Elías F, Sainz-García E, et al. Atmospheric plasma-polymerization of hydrophobic and wear-resistant coatings on glass substrates. Surf Coatings Technol. 2014;259:374–385.
[7] Yim JH, Rodriguez-Santiago V, Williams AA, et al. Atmospheric pressure plasma enhanced chemical vapor deposition of hydrophobic coatings using fluorine-based liquid precursors. Surf Coatings Technol. 2013;234:21–32.
[8] Chattopadhyay S, Huang YF, Jen YJ, et al. Anti-reflecting and photonic nanostructures. Mater Sci Eng R Reports. 2010;69(1–3):1–35.
[9] Farhadi S, Farzaneh M, Kulinich SA. Anti-icing performance of superhydrophobic surfaces. Appl Surf Sci. 2011;257:6264–6269.
[10] Raut HK, Ganesh VA, Nair AS, et al. Anti-reflective coatings: a critical, in-depth review. Energy Environ Sci 2011;4:3779–3804.
[11] Xue C-H, Jia S-T, Zhang J, et al. Preparation of superhydrophobic surfaces on cotton textiles. Sci Technol Adv Mater. 2008;9:035008.
[12] Zhang X, Shi F, Niu J, et al. Superhydrophobic surfaces: from structural control to functional application. J Mater Chem. 2008;18:621–633.
[13] Jafari R, Farzaneh M. Fabrication of superhydrophobic nanostructured surface on aluminum alloy. Appl Phys A Mater Sci Process. 2011;102:195–199.
[14] Jafari R, Menini R, Farzaneh M. Superhydrophobic and icephobic surfaces prepared by RF-sputtered polytetrafluoroethylene coatings. Appl Surf Sci. 2010;257:1540–1543.
[15] Roach P, Shirtcliffe NJ, Newton MI. Progress in superhydrophobic surface development. Soft Matter. 2008;4:224–240.
[16] Safaee A, Sarkar DK, Farzaneh M. Superhydrophobic properties of silver-coated films on copper surface by galvanic exchange reaction. Appl Surf Sci. 2008;254:2493–2498.
[17] Saleema N, Farzaneh M. Thermal effect on superhydrophobic performance of stearic acid modified ZnO nanotowers. Appl Surf Sci. 2008;254:2690–2695.
[18] Mukhopadhyay SM, Joshi P, Datta S, et al. Plasma assisted surface coating of porous solids. Appl Surf Sci. 2002;201:219–226.
[19] Zhang J, Van Ooij W, France P, et al. Investigation of deposition rate and structure of pulse DC plasma polymers. Thin Solid Films. 2001;390:123–129.
[20] Zhang F, Sautter K, Larsen AM, et al. Chemical vapor deposition of three aminosilanes on silicon dioxide: surface characterization, stability, effects of silane concentration, and cyanine dye adsorption. Langmuir. 2010;26:14648–14654.
[21] Masuko M, Miyamoto H, Suzuki A. Shear strength and durability of self assembled monolayer. Proc ASME/STLE Int Jt Tribol Conf; Oct 22–24; San Diego, CA; 2007. p. 97–99.
[22] Kilpi L, Ylivaara OMEOME, Vaajoki A, et al. Microscratch testing method for systematic evaluation of the adhesion of atomic layer deposited thin films on silicon. J Vac Sci Technol A Vacuum, Surfaces, Film. 2016;34:01A124.
[23] Trinh QH, Lee SB, Mok YS. Hydrophobic coating of silicate phosphor powder using atmospheric pressure dielectric barrier discharge plasma. Am Inst Chem Eng. 2014;60:829–838.
[24] Borges JN, Belmonte T, Guillot J, et al. Functionalization of copper surfaces by plasma treatments to improve adhesion of epoxy resins. Plasma Process Polym. 2009;6:S490–S495.
[25] Gubala V, Gandhiraman RP, Volcke C, et al. Functionalization of cycloolefin polymer surfaces by plasma-enhanced chemical vapour deposition: comprehensive characterization and analysis of the contact surface and the bulk of aminosiloxane coatings. Analyst. 2010;135(6):1375–1381.
[26] Juda W. Preparation of ion exchange membranes. J Appl Polym Sci. 1953;5193:875–884.
[27] Volcke C, Gandhiraman RP, Gubala V, et al. Plasma functionalization of AFM tips for measurement of chemical interactions. J Colloid Interface Sci. 2010;348:322–328.
[28] Volcke C, Gandhiraman RP, Gubala V, et al. Reactive amine surfaces for biosensor applications, prepared by plasma-enhanced chemical vapour modification of polyolefin materials. Biosens Bioelectron. 2010;25:1875–1880.
[29] Howarter JA, Youngblood JP. Surface modification of polymers with 3-aminopropyltriethoxysilane as a general pretreatment for controlled wettability. Macromolecules. 2007;40:1128–1132.
[30] Liu Y, Li Y, Li XM, et al. Kinetics of (3-aminopropyl)-triethoxylsilane (APTES) silanization of superparamagnetic iron oxide nanoparticles. Langmuir. 2013;29:15275–15282.
[31] Loch CL, Ahn D, Chen C, et al. Sum frequency generation studies at poly(ethylene terephthalate)/silane interfaces: hydrogen bond formation and molecular conformation determination. Langmuir. 2004;20:5467–5473.
[32] Fanelli F, Lovascio S, D'Agostino R, et al. Ar/HMDSO/O_2 fed atmospheric pressure DBDs: thin film deposition and GC-MS investigation of by-products. Plasma Process Polym. 2010;7:535–543.
[33] Alba-Elías F, Ordieres-Meré J, González-Marcos A. Deposition of thin-films on EPDM substrate with a plasma-polymerized coating. Surf Coatings Technol. 2011;206:234–242.
[34] Schäfer J, Foest R, Quade A, et al. Carbon-free SiO_x films deposited from octamethylcyclotetrasiloxane (OMCTS) by an atmospheric pressure plasma jet (APPJ). Eur Phys J D. 2009;54:211–217.
[35] Rombaldoni F, Mossotti R, Montarsolo A, et al. Thin film deposition by PECVD using HMDSO-O_2-Ar gas mixture on knitted wool fabrics in order to improve pilling resistance. Fibers Polym. 2008;9:566–573.
[36] Gueye M, Gries T, Noël C, et al. Interaction of (3-aminopropyl)triethoxysilane with pulsed Ar–O_2 afterglow: application to nanoparticles synthesis. Plasma Chem Plasma Process. 2016;36:1031–1050.
[37] Finot E, Roualdes S, Kirchner M, et al. Surface investigation of plasma HMDSO membranes post-treated by CF_4/Ar plasma. Appl Surf Sci. 2002;187:326–338.
[38] Zanini S, Massini P, Mietta M, et al. Plasma treatments of PET meshes for fuel-water separation applications. J Colloid Interface Sci. 2008;322:566–571.
[39] Li Y, Zhang J, Zhu S, et al. Biomimetic surfaces for high-performance optics. Adv Mater. 2009;21:4731–4734.